

# *Using 3D-printed analogues to investigate the fall speeds and orientations of complex ice particles*

Article

Published Version

Creative Commons: Attribution-Noncommercial-No Derivative Works 4.0

Open Access

Westbrook, C. D. ORCID: <https://orcid.org/0000-0002-2889-8815> and Sephton, E. K. (2017) Using 3D-printed analogues to investigate the fall speeds and orientations of complex ice particles. *Geophysical Research Letters*, 44 (15). pp. 7994-8001. ISSN 0094-8276 doi: [10.1002/2017gl074130](https://doi.org/10.1002/2017gl074130) Available at <https://centaur.reading.ac.uk/71730/>

It is advisable to refer to the publisher's version if you intend to cite from the work. See [Guidance on citing](#).

To link to this article DOI: <http://dx.doi.org/10.1002/2017gl074130>

Publisher: American Geophysical Union

All outputs in CentAUR are protected by Intellectual Property Rights law, including copyright law. Copyright and IPR is retained by the creators or other copyright holders. Terms and conditions for use of this material are defined in the [End User Agreement](#).

[www.reading.ac.uk/centaur](http://www.reading.ac.uk/centaur)

**CentAUR**

Central Archive at the University of Reading

Reading's research outputs online

## Key Points:

- Three-dimensional-printing techniques are used to generate ice particle analogues for geometries such as bullet rosettes and aggregates
- Terminal velocity and fall orientation were measured for analogues falling at same Reynolds number as ice particles in air
- The data are used to test the accuracy of ice fall speed parameterization

## Supporting Information:

- Supporting Information S1
- Table S1
- Data Set S1

## Correspondence to:

C. D. Westbrook,  
c.d.westbrook@reading.ac.uk

## Citation:

Westbrook, C. D. and E. K. Sephton (2017), Using 3-D-printed analogues to investigate the fall speeds and orientations of complex ice particles, *Geophys. Res. Lett.*, 44, doi:10.1002/2017GL074130.

Received 11 MAY 2017

Accepted 18 JUL 2017

Accepted article online 25 JUL 2017

## Using 3-D-printed analogues to investigate the fall speeds and orientations of complex ice particles

C. D. Westbrook<sup>1</sup>  and E. K. Sephton<sup>1</sup> 

<sup>1</sup>Department of Meteorology, University of Reading, Reading, UK

**Abstract** The terminal velocity  $v_t$  and preferred orientations of ice particles have been investigated using 3-D-printed analogues sedimenting in glycerine solutions at Reynolds numbers typical of natural ice particles falling in air. Twenty-two different particle geometries were investigated: these included both simple shapes, such as hexagonal plates, and more complex particles, such as bullet rosettes, plate polycrystals, and aggregates. Two widely used prescriptions for ice particle fall speed were tested against the new experimental data, to determine the accuracy of their predictions. We show that for open particles, such as bullet rosettes and aggregates, one of these prescriptions systematically overestimates  $v_t$ , by as much as 80%.

### 1. Introduction

The sedimentation of ice particles is a fundamental microphysical process. The terminal velocity  $v_t$  of ice crystals is important for climate because it determines the lifetime of cirrus clouds and influences vertical transport of water vapor in the upper troposphere, modulating the top of atmosphere radiation budget. Sanderson *et al.* [2008] and Mitchell *et al.* [2008] have shown that the fallout rate of ice crystals in these clouds is one of the largest sensitivities in current climate models. Meanwhile, precipitation rate is proportional to the terminal velocity of the particles, implying quantitative forecasts of this quantity require accurate snowflake terminal velocities. Ice sedimentation is also a key variable for the evolution of the individual crystals themselves, influencing all of the key microphysical processes including vapor growth and evaporation, riming, aggregation, and melting [Pruppacher and Klett, 1997].

A number of prescriptions have been proposed for calculating the fall speed of an ice particle based on its physical properties (specifically mass  $m$ , maximum dimension  $D$ , and projected area  $A$ ), including Mitchell [1996], Khorostyanov and Curry [2005], and Mitchell and Heymsfield [2005] (from now on collectively referred to as MHKC), and references therein. Fundamentally, these approaches involve relating the dimensionless Best number  $X$  (or equivalently drag coefficient  $C_D = X/Re^2$ ) to the Reynolds number of the particle  $Re$ . Since  $Re$  is a function of  $v_t$ , but  $X$  depends only on  $m, D, A$  (and the properties of the fluid), knowing  $Re(X)$  allows  $v_t$  to be predicted for a given particle. Most recently, Heymsfield and Westbrook [2010, hereafter HW] collected together experimental data from across the published literature to test these schemes. They concluded that the MHKC methods systematically overestimated  $v_t$  for particles where the area ratio  $A_r = A/\frac{\pi}{4}D^2$  was small and proposed their own refined method. Their analysis draws heavily on “analogue” experiments [e.g., List and Schemenauer, 1971; Kajikawa, 1971] where scaled-up metal models of ice particles were dropped in tanks of glycerine and salt solutions to fall at the same Reynolds numbers as ice crystals falling in the atmosphere. Because of dynamic similarity, the relationship between  $X$  and  $Re$  for the model falling in the viscous liquid is the same as for an ice crystal of the same shape falling in air. The advantage of these experiments is that it is possible to make rather accurate measurements of  $X$  and  $Re$  in the controlled laboratory conditions, where the particles have precisely known sizes and shapes, the fall speeds are very slow (order  $\text{cm s}^{-1}$ ), and the particles are large and easily handled. However, a key limitation is the range of particle shapes for which data are available. In particular, there has so far been no data for spatial particles like bullet rosettes, planar polycrystals, and aggregates—yet observations show that these are exactly the particle types which are most prevalent in the atmosphere [e.g., Jiusto and Weickmann, 1973; Korolev *et al.*, 2000; Field and Heymsfield, 2003].

To address this, HW compared their fall speed predictions against various field observations of more complex natural ice particles falling through the air. Such observations represent a much more challenging

©2017. The Authors.

This is an open access article under the terms of the Creative Commons Attribution-NonCommercial-NoDerivs License, which permits use and distribution in any medium, provided the original work is properly cited, the use is non-commercial and no modifications or adaptations are made.

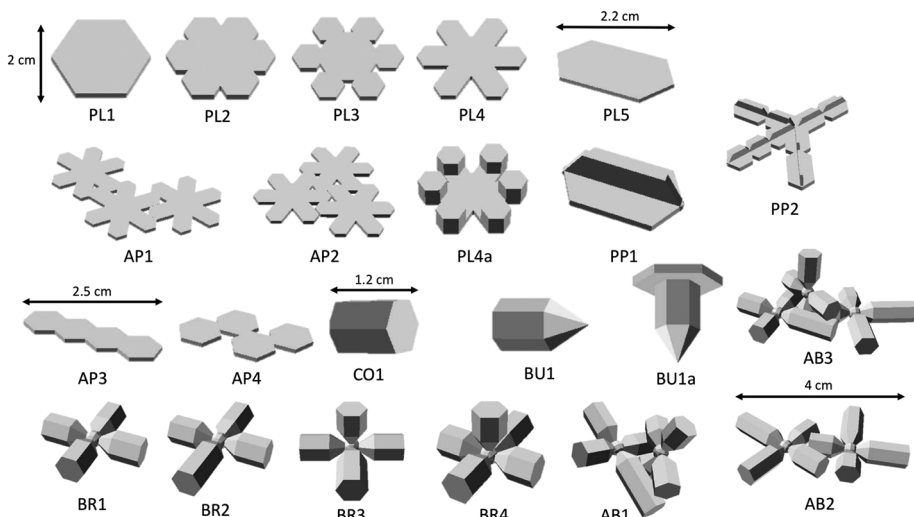


**Figure 1.** Ice particle geometries used in the experiments.

experiment—the particles are small, fragile, easily blown by the wind, and may melt/evaporate while being handled. HW calculated the ratio of the predicted fall speed using their method  $v_t^p$  to the measured fall speed  $v_t^m$ . They found that the median value of  $v_t^p/v_t^m$  for a given particle size was close to 1 (their Figure 6d), indicating that the predicted values match the measurements *on average*. However, the individual data points are highly scattered ranging from  $\approx 0.5$  to 2 at all sizes (i.e., discrepancies of a factor of 2). This raises an important question: does this scatter arise because the HW method has factor of 2 errors for certain complex particle shapes? or does it arise because the field data have factor of 2 uncertainties in them?

To answer this question, and to test the accuracy of both the HW and MHKC predictions, we have revived the analogue method for measuring  $X$ - $Re$  relationships. However, whereas the model particles in those original experiments were machined by hand (leading to relatively simple shapes and few of them), the new idea in the present paper is to exploit recent developments in 3-D-printing technology to manufacture a range of more complex and realistic particle shapes, including polycrystals and aggregates, which can be used to test fall speed parameterizations more rigorously, and determine the accuracy of the HW and MHKC approaches.

## 2. Experimental Methods

### 2.1. Fabrication of Ice Analogue

The analogues were manufactured using the fused filament fabrication technique. Melted plastic (Polylactic acid, PLA) is extruded from a small nozzle (0.4 mm in diameter). The nozzle is scanned along two horizontal axes and deposited onto a glass plate, forming a thin layer of plastic of arbitrary shape. The plate is then moved down, and the process is repeated, with the particle thus being built up in a series of thin (0.06 mm) layers.

The geometry of the particles was designed using an open-source computer-aided design package (OpenSCAD, [www.openscad.org](http://www.openscad.org)). The shapes of the particles that we constructed are shown in Figure 1. The range of particle types is much broader than previous analogue experiments, including polycrystals (bullet rosettes and plate-like polycrystals) and aggregates, as well as simpler monocrystal geometries (which nonetheless are more elaborate than previous work, including scalene geometries, a bullet crystal with a plate cap, and branched planar crystal with columns growing from the tips). Some aspects of the geometry remain idealized (such as the 90° angles between the bullets in the bullet rosettes)—typically, these idealizations were made to simplify the process of producing a successful print. However, we feel that these are logical first steps to mimicking natural polycrystals and aggregates.

The particle shapes were converted into a set of instructions for the printer using standard open-source “slicer” software (Cura, <https://ultimaker.com/en/products/cura-software>).

### 2.2. Measurements of Terminal Velocity and Derivation of $Re$ and $X$

The particles were dropped in a cylindrical tank 28 cm in diameter and 63 cm in height, which was filled with known volumes of glycerine and water to produce mixtures of 0–85% by volume. The time taken to fall a

fixed distance through the tank was used to estimate  $v_t$ . Sampling at the very top and bottom of the tank was avoided, to allow the particles time to accelerate to terminal velocity after their release at the top and to avoid any distortions in the flow field as the particle approached the rigid bottom of the tank. Sensitivity tests using different fall distances gave the same results, indicating that we were indeed sampling the particles at their terminal velocity.

Particle area, maximum dimension, and volume were taken from the OpenSCAD design; however, we also checked these against measurements of the particle dimensions using Vernier calipers. Sometimes, there were small differences, and we rescaled the relevant parameters accordingly.

To parameterize the terminal velocity of a particle as a function of its size and shape (along with known fluid parameters), we need to characterize the relationship between  $X$  and  $Re$ . The Reynolds number is given by  $Re = v_t D \rho_{\text{fluid}} / \eta$ , where  $\eta$  is the dynamic viscosity of the fluid and  $\rho_{\text{fluid}}$  is the density of the fluid. Therefore,  $Re$  can be straightforwardly determined from the measured terminal velocity, knowing the size of the analogue, and fluid density and viscosity data which can be calculated to within a few percent using the method of Cheng [2008], from the fraction of glycerine in the solution and its temperature. We estimate that  $Re$  should be accurate to within approximately 5% typically.

Atmospheric ice particles span a wide range of  $Re$ . For example, a small 200  $\mu\text{m}$  crystal falling at 0.1  $\text{ms}^{-1}$  in a cirrus cloud has a Reynolds number of  $\sim 1$ , while a large 5 mm snowflake falling at 1  $\text{ms}^{-1}$  near the ground has a Reynolds number of  $\sim 500$ . Varying the fraction of glycerine in the tank allowed us to sample data points across this range.

At terminal velocity, the weight of the particle, less the weight of the fluid displaced, is equal to the drag force  $= \frac{1}{2} C_D \rho_{\text{fluid}} v_t^2 A$ . Therefore, the drag coefficient  $C_D$  can be determined from the measured terminal velocity of the particle, along with knowledge of the fluid and particle properties

$$C_D = \frac{2gV\Delta\rho}{\rho_{\text{fluid}}v_t^2A} \quad (1)$$

where  $V$  is the volume of the particle,  $\Delta\rho = (\rho_{\text{particle}} - \rho_{\text{fluid}})$ , and  $g$  is the acceleration due to gravity. Note here the linear dependence on  $(\Delta\rho) / \rho_{\text{fluid}}$ . Because  $(\Delta\rho) < \rho_{\text{fluid}}$  in our case, this means that small errors in our knowledge of the particle (and fluid) density can propagate into large fractional errors in  $C_D$ . The density of the fluid can be determined quite accurately from the density of glycerine, water, and the volume fraction of each in the mixture (note that there is a typographical error in equation 25 of the Cheng paper: to compute the density of the mixture, one should use the glycerine fraction by volume and not by mass). The density of the PLA filament used in the print process is specified by the manufacturer as 1240  $\text{kg m}^{-3}$ . However, no error bar is provided on this value, and it is not clear whether the density of the printed analogues is equal to that of the original filament before melting. Therefore, we conducted a series of “sink/float” tests. Using solutions of different volume fractions of glycerine and water, we determined the point at which the analogues transitioned from sinking to floating. Since the density of each solution can be computed, the density of the plastic analogues was estimated to be  $1252 \pm 3 \text{ kg m}^{-3}$ .

Once we have the drag coefficient,  $X$  can be computed as  $X = C_D Re^2$ . We parameterized  $Re$  as a function of a “modified best number”  $X^* = X \times A_r^{0.5}$ : again, this is easily computed.

### 2.3. Validation of Experimental Procedures Using Particles of Known Drag Coefficient (Thin Circular Discs) As A Reference

To validate the experimental procedure set out above, Figure 2 shows  $X$  and  $Re$  measurements for thin circular discs (thickness 1.5 mm; diameters of 15, 20, and 25 mm) for a wide range of Reynolds numbers ranging from  $Re \approx 0.1 - 1000$  using glycerine solutions ranging from 0 to 85%. Overlaid are data from previous laboratory measurements for thin discs from Jayaweera [1965], Kajikawa [1971], and Willmarth *et al.* [1964]. Also plotted is the theoretical result of Roscoe [1949] for a thin disc of aspect ratio 0.1, which is valid for  $Re \lesssim 1$ . Our data are in close agreement with these previous studies, and theory, to within  $\approx 10\%$ . We take this figure as an estimate of the likely uncertainty for our results that follow in section 3.

We note that near  $Re = 100$  our data points fall slightly lower (smaller  $Re$  for a given  $X$ ) than those of Jayaweera [1965] and Kajikawa [1971], by  $\approx 20\%$ . Jayaweera [1965] comments that in his experiments the measured drag became somewhat sensitive to the detailed aspect ratio and density of the disc near  $Re = 100$ , which he attributes to the onset of unsteady fluid flow around the particle. The density of our discs was considerably

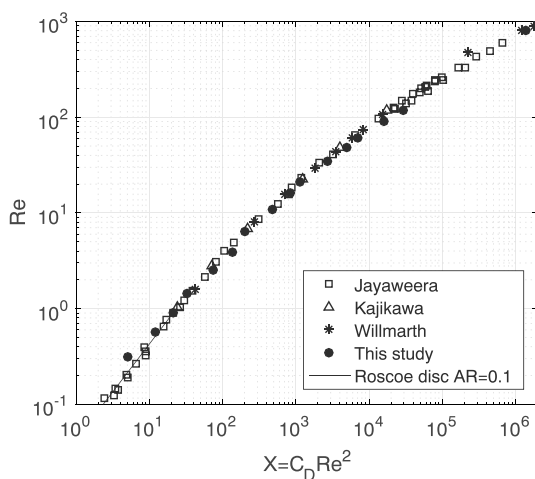


**Figure 2.** Measurements of  $Re$  and  $X$  for discs, compared against previous laboratory measurements (symbols) and theory (line).

lower than his, and we suspect this to be the origin of the difference. This highlights a limitation of analogue experiments: the dynamic similarity between the models in the tank and ice crystals in the atmosphere is only strictly valid when the particles are falling steadily, such that the flow pattern is entirely controlled by  $Re$ . At low  $Re$  the similarity holds because the particles fall stably, and oscillations are damped; but for large  $Re$  the particles start to flutter and tumble (typically at  $Re > 100$ ) [Willmarth *et al.*, 1964], and in this regime the dynamic similarity becomes less accurate, because other parameters (such as the density of the particle relative to the fluid) also play a rôle. In what follows we will present some data with  $Re > 100$  but emphasize that some care is needed in its interpretation.

### 3. Results for Realistic Ice Particle Shapes

We have divided our results into three categories: (a) relatively simple monocrystals which comprise habits like hexagonal plates (PL1), branched planar crystals (PL2–PL4), a scalene plate (PL5), branched plate with columns (PL4a), a solid column of aspect ratio 1.2 (CO1), and the bullet and capped bullet (BU1 and BU1a); (b) polycrystals, including the bullet rosettes (BR1–BR4), crossed plate (PP1), and radiating plates (PP2); and (c) aggregates, with bullet rosette (AB1–AB3), plate (AP3 and AP4), or branched planar (AP1 and AP2) monomers.

All of the particles fell in a well-defined orientation, and this orientation is illustrated in Figure 1 (viewpoint is an observer looking downward on the falling particle at approximately 45° from nadir, with the exception of BU1a which is viewed looking upward at 45°). Broadly speaking, the models settled in orientations where their maximum dimension was in the horizontal plane. This rule of thumb was not entirely universal however, for example, particle AB1 had its axis of longest span inclined at an angle from the horizontal plane.

As  $Re$  increased above  $\sim 100$ , some of the particles began to oscillate gently as they fell: video recordings were made, and details of these motions are given below. In all cases this fluttering was of limited angular extent ( $\lesssim 15^\circ$  for all data points shown here); none of the particles tumbled.

For each data point  $X$  we generated a predicted Reynolds number using both the MHKC and HW relationships. We then compared this against the measured  $Re$  to determine the fractional error in the predicted  $v_t$ . Note that each  $(X, Re)$  pair is derived from the average of five individual measurements. The variability in  $v_t$  from run to run was 5% or less.

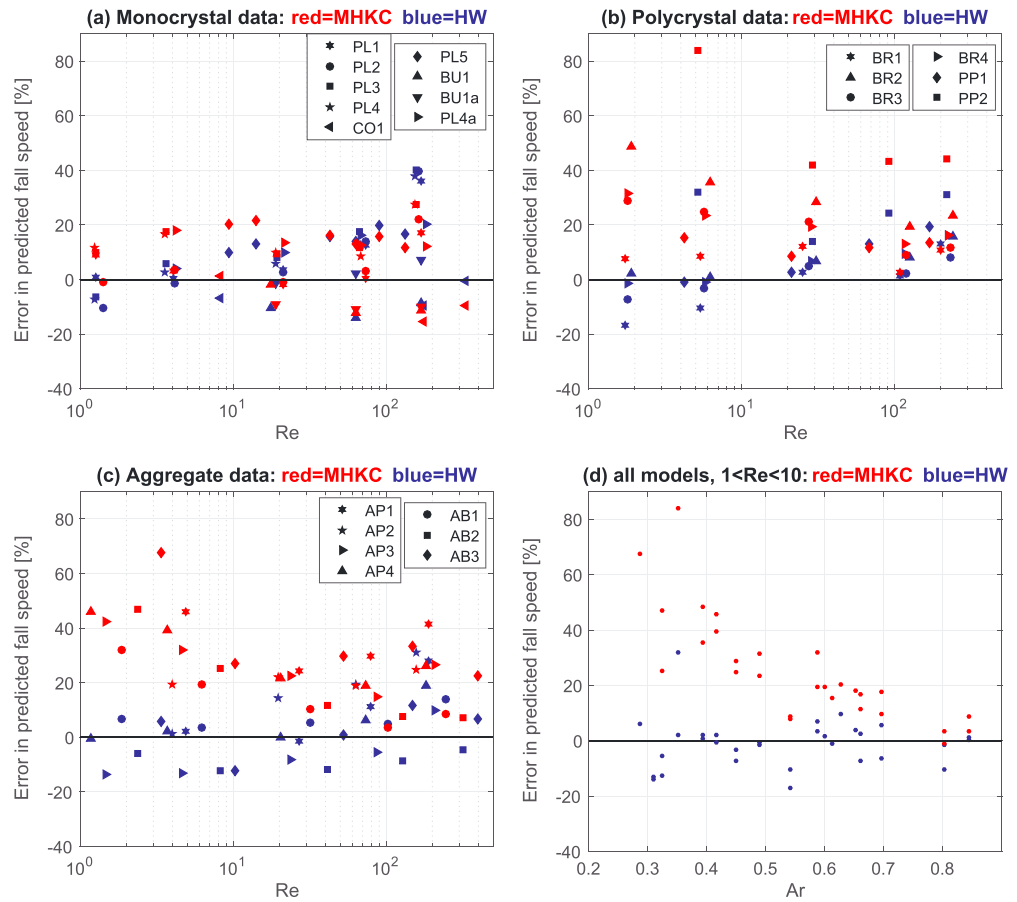
The three MHKC studies give almost identical results for the Reynolds numbers considered here: in what follows we use the equations in Mitchell [1996].

Figure 3 shows the error in terminal velocity that would be obtained using the MHKC (red markers) and HW (blue markers) prescriptions, as a function of Reynolds number. Errors are given as percentages of the true (measured) value; positive values indicate that the prescription is overestimating the particle fall speed.

#### 3.1. Monocrystals

Figure 3a shows the error in  $v_t$  predicted by the HW and MHKC methods for monocrystals. We begin by investigating a simple hexagonal column CO1. Both MHKC and HW provide realistic estimates of  $v_t$  for this shape, with errors of  $< 15\%$  in both cases. Next we consider the bullet (BU1) and a bullet with plate cap (BU1a). Again,  $v_t$  is well predicted by both methods, to within  $\approx 10\%$ . CO1 and BU1 fell stably, with the long axis of the column/bullet horizontally oriented at all  $Re$ . BU1a fell with the capping plate in the horizontal plane, and the tip of the bullet pointed vertically downward; again, no significant oscillations were observed.

Next we consider thin hexagonal plates and branched planar crystals (PL1–PL4). Similar shapes were analyzed by List and Schemenauer [1971]. For  $Re < 100$ , MHKC and HW both provide realistic estimates of the particle fall speed, to within  $\pm 20\%$ . However, for the run at  $Re \approx 150$ , larger differences are observed between the



**Figure 3.** Fractional error in predicted fall speeds for the various particle shapes investigated for (a) monocrystals, (b) polycrystals, and (c) aggregates, as a function of  $Re$ . Legend shows key to particle shapes; red markers are comparison against MHKC method; blue markers are comparison against HW method. Positive values are where the chosen method overestimates  $v_t$ . (d) Error as a function of area ratio for low Reynolds number ( $1 < Re < 10$ ), highlighting the bias in MHKC for particles with open geometries.

measurements and predictions: up to +30% for MHKC and +40% for HW. Given the similarity of these simple plate-like particles to discs, we suspect that this difference is a manifestation of the same phenomenon discussed in section 2.3—further experiments with different particle/fluid density ratios are required to test this hypothesis. The particles fell with their major axes horizontal, and even at  $Re = 150$  only a very slight rocking motion was detected.

The plate with columns PL4a was captured reasonably well by both methods, with both MHKC and HW overestimating  $v_t$  slightly, but by no more than 20%. The particle oriented itself such that the column extensions pointed upward. No significant fluttering was observed even at  $Re = 200$ .

### 3.2. Polycrystals

In situ evidence has shown that most ice particles nucleated at temperatures below  $\approx -20^\circ\text{C}$  are polycrystalline. In cirrus clouds these often take the form of bullet rosettes. Our model rosettes have four to five arms, oriented at  $90^\circ$  to one another. Model BR1 is the simplest geometry with all four arms of equal length, lying in the same plane. Model BR2 is an elaboration where one of the arms has been extended to be 20% longer than the other three. Model BR3 is the same as BR2 except that the long arm is rotated such that it lies at  $90^\circ$  to the plane formed by the three shorter arms. Finally, BR4 has the same geometry as AB1 but with a fifth arm extending out of the plane.

Figure 3b shows that the HW method accurately predicts the fall speeds of these rosette particles, to within  $\approx 15\%$ . The MHKC approach has a poorer accuracy for these particles, particularly at low Reynolds number. At  $Re = 2$  the fall speeds are overpredicted by 50% for BR2 and 30% for BR3 and BR4. This low Reynolds number

regime is very relevant for cirrus clouds where the particles are typically only a few hundred microns in size. Predictions for the fall speed of BR1 are much better: less than 10% at all  $Re$ . We note that the largest errors for MHKC are for the rosettes with the lowest area ratio (0.39 for BR2 versus 0.55 for BR1).

BR1 fell stably with its arms in the horizontal plane; although for the run at  $Re = 200$  a weak fluttering motion was observed as the particle fell. Model BR2 also fell with its arms in the horizontal plane, despite its asymmetrical geometry. BR3 fell with three arms close to horizontal but slightly inclined, as though the long arm was experiencing greater drag. The short arm orthogonal to the other three was oriented upward. Both BR2 and BR3 fell very stably. BR4 fell with four arms in the horizontal plane and one arm vertical—at high  $Re$  this model fluttered noticeably more than the others, rocking back and forth by approximately 10°.

In addition to rosettes, plate-like polycrystals may also occur. The geometry of these particles is often rather complicated. We investigated two idealizations: particle PP1 is a “crossed plate” and is essentially particle PL5 with an additional half plate attached at right angles on one face; particle PP2 is a more elaborate “radiating plate.” Both are loosely based upon imagery in *Kikuchi et al. [2013]* (their Figure 1: CP4a and CP4c). The HW method captures the fall speed of PP1 rather accurately, with agreement to within 10% at all  $Re$ . MHKC also provides realistic estimates of  $v_t$  for this particle, with the largest error being 15% at  $Re = 5$ . The fall speeds for particle PP2 are not so accurately predicted. Errors of up to 30% were found for the HW method, while MHKC overpredicts the fall speed of this particle by 40–70%. It is not clear to us why this particular geometry stands out from the other data (particularly at low  $Re$ )—in future work we would like to investigate this systematically using other realizations of plate polycrystal structures. We do note, however, that this particle has one of the smallest area ratios of the data set (0.35).

In terms of orientations, the crossed plate oriented itself such that the complete plate was horizontal and the protruding fin was pointed vertically upward, in an analogous way to the orientation of the plate with columns PL4a. The radiating branches in PP2 were oriented horizontally; again, the “fins” were pointed upward. Both models showed a greater tendency to oscillate at high  $Re$  than the other models, with flutter angles up to 15° observed at  $Re = 200$ .

### 3.3. Aggregates

As ice particles fall through the atmosphere, they come into contact with one another and may form aggregates. We constructed seven aggregate analogues, intended to represent those found in different conditions.

First, we consider aggregates of bullet rosettes, models AB1–AB3. Each of these is essentially connected arrangements of the single rosettes discussed earlier. To ensure mechanical stability, the rosettes were designed so that the monomers overlapped in space very slightly at the point of contact, and when printed, this led to secure connections between the monomers. Models AB1 and AB2 have two rosette monomers arranged in different ways (AB2: two rosettes of type BR2 lying in the same plane and AB1: one rosette of type BR1 and another of type BR2 arranged at right angles, with connections on two pairs of arms). Model AB3 contains three monomers of types BR1 and BR2.

The fall speeds of the rosette aggregates are predicted rather accurately by HW, with errors of  $\approx 10\%$  typically. The fall speeds predicted by MHKC meanwhile are much less accurate:  $v_t$  is overestimated by 70% for model AB3 at  $Re = 3$ , falling to 30% at  $Re = 50$ . For AB2 the errors are 45% at  $Re = 2.5$ , falling to 10% at  $Re = 40$ . The errors for AB1 are more modest (30% at  $Re = 2$  and 10% at  $Re = 30$ ). The overestimation of  $v_t$  follows the same pattern as for the rosettes individually: the largest biases in MHKC are for the lowest area ratios (0.29 for AB3 and 0.33 for AB2, compared to 0.58 for AB1).

The two monomers of AB1 were oriented in the form of a “v” shape with apex down as the particle fell. The fall motion was quite stable over the range of  $Re$  considered; however, a slow rotation around the vertical axis was observed. Model AB2 fell with the arms of the rosettes lying in the horizontal plane; at  $Re = 300$  a gentle fluttering motion was observed but over a very small range of angles (<5%). AB3 fell with the two monomers of type BR2 in the horizontal plane; at  $Re = 400$  oscillations were observed, of about 10° amplitude.

Next we consider aggregates of branched planar crystals, AP1 and AP2. These are formed of three monocrystals of type PL4 arranged in the same plane and crudely mimic “early aggregates” of stellar/dendrite crystals (see HW, and references therein). HW predicts  $v_t$  for these particles quite accurately for  $Re < 100$ , with errors of at most 15%. MHKC produces larger errors, up to 45% for model AP1 at  $Re = 6$ . Again, this is a model with a rather low area ratio (0.35). For  $10 < Re < 100$  MHKC consistently overestimates  $v_t$ , by around 25%. For  $Re > 100$

both methods overestimate  $v_t$ , by  $\approx 30\%$ . Both AP1 and AP2 were observed to fall very stably, and even at  $Re=150$  no significant fluttering was observed.

Finally, we consider chain-like aggregates of plates and models AP3 and AP4. Such chains are often observed in electrified anvil clouds, where the strong electric field is believed to influence the aggregation process [Connolly *et al.*, 2005]. The HW method predicts  $v_t$  for these particles to within 20% at all  $Re$ . MHKC overestimates  $v_t$  by 45% at  $Re=1.5$ , falling to 20% overestimation at  $Re=20$ . The models fell with their plate monomers in the horizontal plane—at high  $Re$  model AP3 fluttered a little around its length as it fell; no such oscillations were evident for the staggered chain AP4.

### 3.4. Sensitivity to Area Ratio

From the limited experimental data available to them, HW argued that MHKC's method led to  $v_t$  being overestimated when the area ratio was low, i.e., when the geometry of the particle projection is very open (like an aggregate), rather than compact (like a short column), and that this error was largest at low  $Re$ . Our results seem to indicate the same behavior is valid for a broad range of ice particle geometries. To probe this sensitivity more directly, Figure 3d shows all of the 22 particle types combined into a single plot, this time with the abscissa representing the area ratio  $A_r$ ; now only data with low Reynolds number, between 1 and 10, are shown. This shows the behavior anticipated by HW very clearly: the blue data points (error in HW method) are clustered close to 0% and show no clear trend with  $A_r$ . By contrast, the red data points (error in MHKC) indicate very large (up to 80%) errors at  $A_r=0.3$ , falling to near zero for  $A_r > 0.8$ .

## 4. Conclusions

We have revived the analogue method of determining ice particle drag coefficients, using modern 3-D-printing techniques to fabricate a much broader range of more realistic analogues, including polycrystals and aggregates for which no data were previously available. New measurements of  $Re$  and  $X$  and the preferred orientations of the particles have been presented. We confirm HW's suggestion that the formulae given by MHKC overestimate  $v_t$  substantially when  $A_r$  is low, particularly if  $Re$  is also low. The practical significance of these errors depends on the area ratio of natural ice particles in the atmosphere: Mitchell *et al.* [2011] show that this is likely dependent on both the temperature of the cloud and its latitude. We have shown that HW's alternative method gives more robust results: for  $Re < 100$  the predicted fall speeds lie within 20% of the measured ones, for 21 of the 22 particles studied. This suggests that a factor of 2 scatter in  $v_t^p/v_t^m$  shown in HW very likely arises primarily as a result of large errors in the field observations themselves, and not large errors in the HW method, and we suggest that future parameterization efforts should keep these large observational uncertainties in mind.

At  $Re > 100$  the dynamic similarity between our analogue experiments and the atmosphere is less rigorous. Nonetheless, the HW method predicts the fall speeds in this regime quite accurately for most of the particles, the interesting exception being particles which are very thin and flat (PL1–PL4 and AP1 and AP2). More work is needed to understand  $v_t$  in this regime, perhaps by using much smaller analogues falling in air.

The particle shapes considered in our study are much more realistic than previous analogues but still idealized. The 3-D-printing technique opens up new opportunities to manufacture large ensembles of aggregate and polycrystal geometries, based on either detailed process models [Westbrook *et al.*, 2004; Leinonen and Szyrmer, 2015] or analysis of in situ imagery [Um *et al.*, 2008; Kleinkort *et al.*, 2017]. It also makes it possible to alter the parameters of individual particles (e.g., the angles between the bullets in a rosette) in a systematic way to understand in detail how the drag and orientation are controlled.

## References

Cheng, N.-S. (2008), Formula for the viscosity of a glycerol-water mixture, *Ind. Eng. Chem. Res.*, 47, 3285–3288.

Connolly, P., *et al.* (2005), Aircraft observations of the influence of electric fields on the aggregation of ice crystals, *Q. J. R. Meteorol. Soc.*, 131, 1695–1713.

Field, P. R., and A. J. Heymsfield (2003), Aggregation and scaling of ice crystal distributions, *J. Atmos. Sci.*, 60, 544–560.

Heymsfield, A. J., and C. D. Westbrook (2010), Advances in the estimation of ice particle fall speeds using laboratory and field measurements, *J. Atmos. Sci.*, 67, 2469–2482.

Jayaweera, K. O. L. F. (1965), The behaviour of small clusters of bodies falling in a viscous fluid, PhD thesis, Imperial College London. (digitised version available from the British Library, [ethos.bl.uk](http://ethos.bl.uk)).

Jiusto, J. E., and H. K. Weickmann (1973), Types of snowfall, *Bull. Am. Meteorol. Soc.*, 54, 1148–1162.

Kajikawa, M. (1971), A model experimental study on the falling velocity of ice crystals, *J. Meteor. Soc. Jpn.*, 49, 367–375.

## Acknowledgments

We are very grateful to Selena Zito and Rosy Wilson for providing technical support for these experiments and to Andrew Lomas for making the “catcher” to easily remove the model particles from the fluid tank. C.D.W. would like to acknowledge former undergraduate students Ahmad Aljasmi, Hannah Gough, Judith McConnell, Jessica Welford, and Chris Roberts for their efforts in earlier incarnations of this experiment. Thanks also to Paul Debeu for pointing out the error in equation 25 of the Cheng paper. E.K.S. was supported by a bursary from the Undergraduate Research Opportunities Programme at the University of Reading. *Data availability:* stereolithography files for the particle models, along with  $Re$  and  $X$  data for each analogue, can be downloaded as supporting information accompanying this article.

Khvorostyanov, V. I., and J. A. Curry (2005), Fall velocities of hydrometeors in the atmosphere: Refinements to a continuous analytical power law, *J. Atmos. Sci.*, 62, 4343–4357.

Kleinkort, C., et al. (2017), Visual hull method for realistic 3D particle shape reconstruction based on high-resolution photographs of snowflakes in free fall from multiple views, *J. Atmos. Oceanic Technol.*, 34, 679–702.

Kikuchi, K., et al. (2013), A global classification of snow crystals, ice crystals, and solid precipitation based on observations from middle latitudes to polar regions, *Atmos. Res.*, 132–133, 460–472.

Korolev, A. V., et al. (2000), Ice particle habits in stratiform clouds, *Q. J. R. Meteorol. Soc.*, 126, 2873–2902.

Leinonen, J., and W. Szyrmer (2015), Radar signatures of snowflake riming: A modeling study, *Earth Space Sci.*, 2, 346–358.

List, R., and R. S. Schemenauer (1971), Free-fall behavior of planar snow crystals, conical graupel and small hail, *J. Atmos. Sci.*, 28, 110–115.

Mitchell, D. L. (1996), Use of mass- and area-dimensional power laws for determining precipitation particle terminal velocities, *J. Atmos. Sci.*, 53, 1710–1723.

Mitchell, D. L., and A. J. Heymsfield (2005), Refinements in the treatment of ice particle terminal velocities, highlighting aggregates, *J. Atmos. Sci.*, 62, 1637–1644.

Mitchell, D. L., P. Rasch, D. Ivonava, G. McFarquhar, and T. Nousiainen (2008), Impact of small ice crystal assumptions on ice sedimentation rates in cirrus clouds and GCM simulations, *Geophys. Res. Lett.*, 35, L09806, doi:10.1029/2008GL033552.

Mitchell, D. L., S. Mishra, and R. P. Lawson (2011), Representing the ice fall speed in climate models: Results from Tropical Composition, Cloud and Climate Coupling (TC4) and the Indirect and Semi-Direct Aerosol Campaign (ISDAC), *J. Geophys. Res.*, 116, D00T03, doi:10.1029/2010JD015433.

Pruppacher, H. R., and J. D. Klett (1997), *Microphysics of Clouds and Precipitation*, 2nd ed., Kluwer Acad., Netherlands.

Roscoe, R. (1949), The flow of viscous fluids round plane obstacles, *Philos. Mag.*, 40, 338–351.

Sanderson, B. M., et al. (2008), Towards constraining climate sensitivity by linear analysis of feedback patterns in thousands of perturbed-physics GCM simulations, *Clim. Dyn.*, 30, 175–190.

Um, J., et al. (2008), Dimensions and aspect ratios of natural ice crystals, *Atmos. Chem. Phys.*, 15, 3933–3956.

Westbrook, C. D., R. C. Ball, and P. R. Field (2004), A theory of growth by differential sedimentation with application to snowflake formation, *Phys. Rev. E*, 70, 21403.

Willmarth, W. W., N. E. Hawk, and R. L. Harvey (1964), Steady and unsteady motions and wakes of freely falling discs, *Phys. Fluids*, 7, 197–208.